PCCP

Monitoring Aromatic Ring-Currents in Mg-porphyrin by Time-Resolved Circular Dichroism

Journal:	*Physical Chemistry Chemical Physics*
Manuscript ID	CP-ART-09-2020-004815.R1
Article Type:	Paper
Date Submitted by the Author:	27-Oct-2020
Complete List of Authors:	Nam, Yeonsig; University of California Irvine, Chemistry Rouxel, Jeremy; University of California Irvine, Chemistry Lee, Jin Yong; Sungkyunkwan University, Chemistry Mukamel, S.; University of California, Chemistry

ARTICLE

Monitoring Aromatic Ring-Currents in Mg-porphyrin by Time-Resolved Circular Dichroism

Received 00th January 20xx,
Accepted 00th January 20xx

DOI: 10.1039/x0xx00000x

Yeonsig Nam,*[ab†] Jérémy R. Rouxel,*[a†] Jin Yong Lee,*[b] and Shaul Mukamel *[a]

Time-resolved circular dichroism signals (TRCD) in the X-ray regime can directly probe the magnitude and the direction of ring currents in molecules. The electronic ring currents in Mg-porphyrin, generated by coherent superposition of electronic states induced by circularly polarized UV pulse, are tracked by a time-delayed circularly polarized attosecond X-ray pulse. The signals are calculated using the minimal coupling Hamiltonian that directly makes use of transitions current densities. TRCD signals obtained from left and right circularly polarized light pump have opposite signs, revealing the direction of the ring current. Molecular aromaticity and its role in photochemical reactions such as ring opening or closure can be studied using this technique.

Introduction

Exploring and controlling the dynamics of aromatic ring currents has received great attention for decades. Ring currents have been used to quantify the aromaticity of the ring molecules[1-3]. Their magnitude has been compared with nucleus-independent chemical shift[4] or diamagnetic susceptibility exaltation value[5] and used to determine the aromaticity of molecules. Aromatic ring currents and their induced magnetic fields have been recently used for nanodevices[6-10], such as a molecular magnets[6], quantum device[7], photo-switches[9-11], and to generate ultrafast magnetic field pulses[8].

An aromatic ring current is generated by a magnetic field perpendicular to the molecular plane due to the delocalized π electrons[12]. A more effective way to create ring currents using circularly polarized light[6, 13, 14] was suggested by the Manz group: the chirality of the laser pulse is transferred to the molecular system, inducing a clockwise or counterclockwise ring current. This current is much stronger than what can be induced by an external magnetic field with present technology[6]. For example, in a Mg-porphyrin molecule, the net ring current induced by a circularly polarized laser π-pulse correspond to one induced by a magnetic field of 8048 T, which is 100 times higher than the maximum permanent magnetic field currently available[6].

So far, monitoring the ultrafast circular coherent dynamics of ring currents in real time has been a challenge. Many experimental and computational approaches have been developed for the indirect measurement of aromatic ring currents: nuclear magnetic shielding[15, 16], current density[3] and bond order[17], and polarizability analysis[18, 19].

Several studies have attempted the direct observation of aromatic ring currents. Yuan *et al*.[20] and Wollenhaupt *et al*.[21] had measured the molecular angular and energy-resolved photoelectron spectra by using time-delayed X-ray pulses. Neufield *et al*.[22] proposed that high-harmonic generation in the presence of a ring current causes the emission of elliptically polarized harmonics. Koksal *et al*.[23] showed the possible manipulation of a ring current and induced magnetic field by changing the frequency and the orbital angular momentum of the light beams. However, both photoelectron circular dichroism and high-harmonic generation require elaborate experimental setups and are hard to interpret. Here, we discuss the use of time-resolved X-ray circular dichroism (TRCD) to directly measures the fast electronic motions associated with ring currents

Attosecond X-rays pulses provide real-time and real-space resolution of electronic structure enabling the creation of molecular movies[24]. The high-spatial resolution of X-rays can reveal local properties in delocalized aromatic systems.

CD spectra are usually weak signals on top of a large achiral background. Transient CD signals are usually measured on top of a static background. The use of X-rays excitation from valence excited states allows to generate transitions below the pre-edge region, a frequency regime with no or low static background. The absence of static achiral background induces large asymmetry ratio (>100%, eq 10 below) compared to standard CD techniques (few % or less).

In this paper, we study the use of time-resolved circular dichroism (TRCD) signal to probe ring currents: a UV pump pulse induces a ring current and a delayed X-ray probe measures the

[a] *Department of Chemistry, Physics and Astronomy, University of California, Irvine, 92697-2025, USA. E-mail: jrouxel@uci.edu; smukamel@uci.edu; yeonsign@uci.edu*
[b] *Department of Chemistry, Sungkyunkwan University, Suwon, 16419, South Korea. E-mail: jinylee@skku.edu*
† These authors contributed equally to this work.
Electronic Supplementary Information (ESI) available: Details of the TRCD signal calculation, quantum simulation results, stick spectrum, time-dependent density matrix elements and average transition current density. See DOI: 10.1039/x0xx00000x

induced dichroic signal. The magnitude and the sign of the signal reveal the amplitude and the direction of the ring current. We employ the minimal coupling Hamiltonian for the light-matter interaction that expresses the signal directly in terms of transition current densities. Simulations are carried out for Mg-porphyrin where the X-ray probe is tuned to the nitrogen K-edge at 409 eV or to the magnesium K-edge at 1327 eV.

Theory and Computational Details

The time-resolved CD signal

The minimal coupling Hamiltonian for the resonant radiation-matter interaction is (1)

$$H_{\text{int}} = -\int \mathrm{d}\boldsymbol{r}\boldsymbol{j}(\boldsymbol{r})\cdot\boldsymbol{A}(\boldsymbol{r},t)$$

where $\boldsymbol{A}(\boldsymbol{r},t)$ is the electromagnetic vector potential of the incoming field and $\boldsymbol{j}(\boldsymbol{r})$ is the current-density operator: (2)

$$j(r) = \frac{e\hbar}{2mi}[\psi^{\dagger}(r)\nabla\psi(r) - [\nabla\psi^{\dagger}(r)]\psi(r)]$$

where $\psi^{\dagger}(\boldsymbol{r})$ and $\psi(\boldsymbol{r})$ are the electron field creation and annihilation operators at position $\boldsymbol{r}$.

The time-dependent density matrix after two interactions with the pump pulse (Fig. S2) is given by

$$\begin{aligned}\rho_{ee'}(T) &= \langle\langle ee'|\rho(T)\rangle\rangle \\ &= (\frac{-i}{\hbar})^2\int \mathrm{d}r_1\mathrm{d}r_2\mathrm{d}t_1\mathrm{d}t_2 \\ &\langle\langle ee'|j_-(r_2,t_2)j_-(r_1,t_1)|\rho(T-t_1-t_2)\rangle\rangle A^*_{\text{pu}}(r_2,T-t_2)A_{\text{pu}}(r_1,T-t_2-t_1)\end{aligned} \quad (3)$$

$$\begin{aligned}&= (\frac{-i}{\hbar})^2\int \mathrm{d}r_1\mathrm{d}r_2\mathrm{d}t_1\mathrm{d}t_2 \\ &\Big[\langle\langle ee'|\mathcal{G}(t_2)j_{\text{right}}(r_2)\mathcal{G}(t_1)j^{\dagger}_{\text{left}}(r_1)|\rho(t_0)\rangle\rangle A^*_{\text{pu}}(r_2,T-t_2)A_{\text{pu}}(r_1,T-t_2-t_1) \\ &+\langle\langle ee'|\mathcal{G}(t_2)j^{\dagger}_{\text{left}}(r_2)\mathcal{G}(t_1)j_{\text{right}}(r_1)|\rho(t_0)\rangle\rangle A_{\text{pu}}(r_2,T-t_2)A^*_{\text{pu}}(r_1,T-t_2-t_1)\Big]\end{aligned}$$

$\boldsymbol{A}_{\text{pu}}$ is the vector potential of the pump and $\mathcal{G}$ is field free molecular propagator, and $\boldsymbol{j}_-$ denotes the current density superoperator[25]. Here, the subscript left and right indicates the superoperators defined by $O_{\text{left}}\rho = O\rho$ and $O_{\text{right}}\rho = \rho O$.

In the impulsive limit, the density matrix at waiting time T becomes: (4)

$$\rho_{ee'}(T) = -\frac{1}{\hbar^2}\int\frac{\mathrm{d}\omega_1}{2\pi}\frac{\mathrm{d}\omega_2}{2\pi}A_{\text{pu}}(\omega_1)A_{\text{pu}}(\omega_2)$$
$$\left[\frac{j_{e'g}(k_{\text{pu}})\cdot e^*_{\text{pu}}\cdot j^{\dagger}_{eg}(-k_{\text{pu}})\cdot e_{\text{pu}}e^{i(\omega_2-\omega_1)T}}{(\omega_1-\omega_2-\omega_{ee'}+i\Gamma_{ee'})(\omega_1-\omega_{eg}+i\Gamma_{eg})}+\frac{j^{\dagger}_{eg}(-k_{\text{pu}})\cdot e_{\text{pu}}\cdot j_{e'g}(k_{\text{pu}})\cdot e^*_{\text{pu}}e^{-i(\omega_2-\omega_1)T}}{(-\omega_1+\omega_2-\omega_{ee'}+i\Gamma_{ee'})(-\omega_1-\omega_{ge'}+i\Gamma_{ge'})}\right]$$

where $\boldsymbol{e}$ are the electric field polarization vectors which can be left or right polarization. ω_1 and ω_2 run over the bandwidth of the UV pump which is set on resonance with a specific valence excited state. The dephasing rate, $\Gamma = 200\text{cm}^{-1}$, is taken to be the same for all transitions[26].

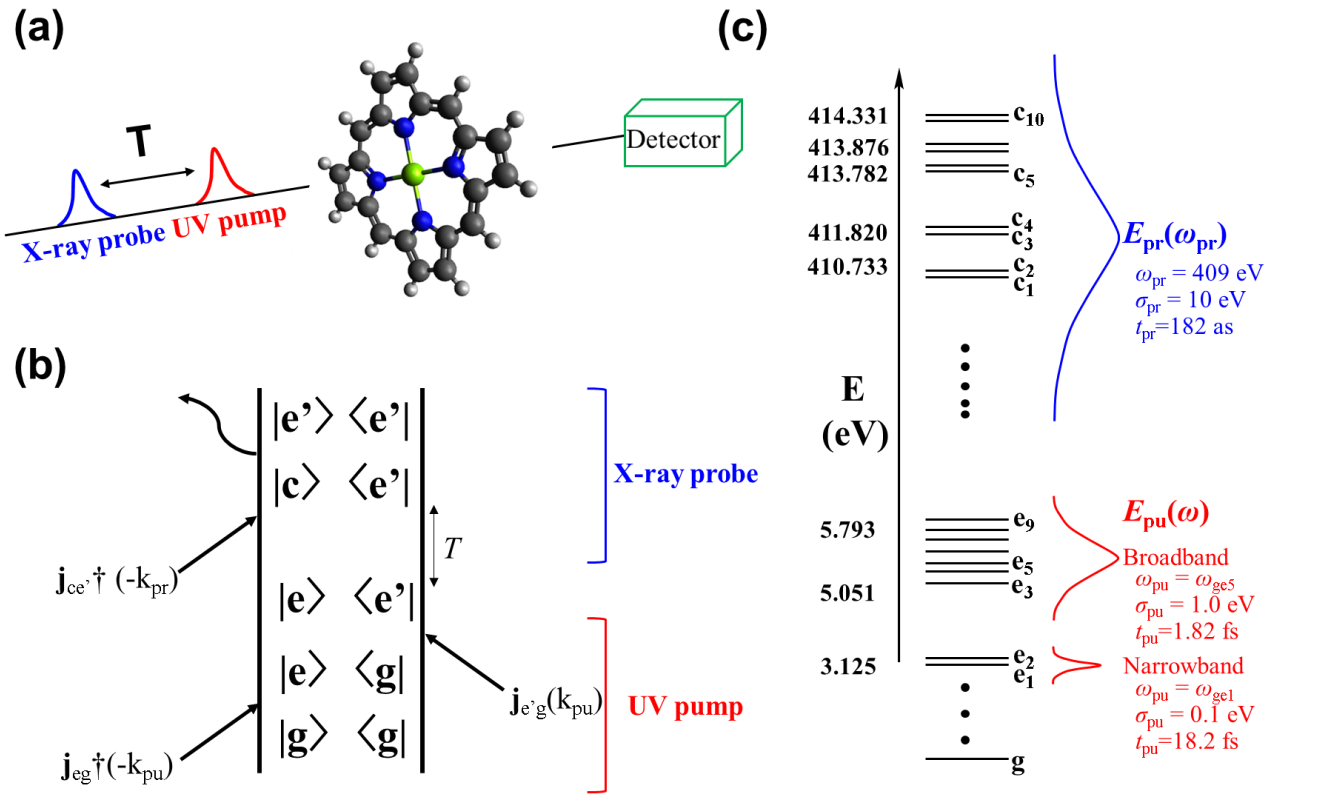

Fig. 1 (a) The Mg-Porphyrin used in this study. Gray, white, blue, and yellow sphere represent carbon, hydrogen, nitrogen, and Mg atom, respectively. (b) Ladder diagram, and (c) the pump/probe setup used to calculate TRCD signal and electronic energy levels contributing to the signal. Valence manifolds are denoted as $\{e_1, e_2, \ldots, e_9\}$ while core excited states are denoted $\{c_1, c_2, \ldots, c_{10}\}$. $\omega_{\text{pu/pr}}$, $\sigma_{\text{pu/pr}}$, and $t_{\text{pu/pr}}$ denotes the central frequency, bandwidth, and the time duration of pump/probe pulse, respectively.

The heterodyne detected signal[27, 28] is given by:

$$S_{\mathrm{CD}}(k_s,\omega_s,T)=\frac{2}{\hbar^2}\mathrm{Re}\int \mathrm{d}r\mathrm{d}t\mathrm{d}r_1\mathrm{d}t_1 A^*_{\mathrm{pr}}(r,t)A_{\mathrm{pr}}(r_1,t-t_1)$$
$$(e^*_L e_L - e^*_R e_R)\langle\langle j(r)|\mathcal{G}(t_1)j_-(r_1)|\rho(t-t_1)\rangle\rangle \quad (6)$$

where Γ indicates the set of pulse parameters, i.e. central frequencies, durations, etc and $\boldsymbol{A}_{\mathrm{pr}}$ is the vector potential of the probe pulse. Expanding to first order in the probe and taking the difference between the left and the right polarizations of the probe we obtain:

$$S_{\mathrm{CD}}(k_s,\omega_s,T)=\frac{2}{\hbar^2}\mathrm{Im}\sum_{ee'c}\int \mathrm{d}t\mathrm{d}t_1 A^*_{\mathrm{pr}}(r,t)A_{\mathrm{pr}}(r_1,t-t_1)\rho_{ee'}(t-t_1)$$
$$\left[j_{e'c}(k_s)\times j^\dagger_{ce}(-k_s)e^{i(\omega_s-\omega_{ce'})t_1-\Gamma_{ce'}t_1} - j^\dagger_{e'c}(-k_s)\times j_{ce}(k_s)e^{i(\omega_s-\omega_{ec})t_1-\Gamma_{ec}t_1}\right] \quad (7)$$

where $\boldsymbol{e}^{a*}_L\boldsymbol{e}^b_L-\boldsymbol{e}^{a*}_R\boldsymbol{e}^b_R=(-i)\boldsymbol{\epsilon}_{abz}$ where $\boldsymbol{\epsilon}_{abz}$ is the Levi-Civita symbol, and summing over electronic eigenstates gives:

where ω_s denote the detection frequency of probe pulse. e and e' denote valence excited states, {e_1, e_2, …, e_9} and c denotes core excited states, {c_1, c_2, …, c_{10}} and $\rho_{ee'}$ is given by Eq. 4. $\boldsymbol{j}_{ce}$ and ω_{ce} refer to the core/valence transition current density matrix elements and the transition frequencies, respectively. × indicates a cross product. The final TRCD expression becomes:

$$S_{\mathrm{CD}}(\omega_s,T)=\frac{2}{\hbar^2}\frac{1}{(2\pi)^2}\mathrm{Re}\sum_{ee'c}A^*_{\mathrm{pr}}(\omega_s)A_{\mathrm{pr}}(\omega_s)\rho_{ee'}(T)$$
$$\left[\frac{j_{e'c}(k_s)\times j^\dagger_{ce}(-k_s)}{\omega_s-\omega_{ce'}+i\Gamma_{ce'}}-\frac{j_{ce}(k_s)\times j^\dagger_{ce'}(-k_s)}{-\omega_s-\omega_{ec}+i\Gamma_{ec}}\right] \quad (8)$$

Details on the TRCD signal derivation can be found in the supporting information.

The pump-probe setup

We assume a left circularly polarized UV pump propagating along the z direction. The Mg-porphyrin molecule (Fig. 1a) is in the xy plane. If the molecule were placed out of this plane, projections of the incoming field polarizations onto the molecular plane would have to be considered without providing extra insights on the ring current dynamics. After a waiting time T, left and right circularly polarized X-ray probes are used to induce the CD signal. Two Gaussian pumps were considered (Fig. 1c): a narrow 0.1 eV bandwidth Fourier-transform-limited pump (central frequency at 3.125 eV, 18.2 fs duration) selectively excites the e_1 or e_2 states and a broad 1.0 eV bandwidth pump (central frequency at 5.400 eV, 1.82 fs duration) excites all valence excited states except e_1 and e_2. The X-ray probe at the N K-edge has a central frequency of 409 eV and 10 eV bandwidth (182 as pulse duration). At the Mg K-edge, we used a 1327 eV central frequency and 10 eV bandwidth (182 as duration).

Electronic structure calculations

Numerical simulations were carried out for Mg-porphyrin (Fig. 1a). Porphyrins are biologically important molecules involved in the primary events of photosynthesis, and biological sensing. It has been used as a model system for the generation of ring currents under an external magnetic field or circularly polarized light. Its aromatic ring currents and induced magnetic field with spectroscopic properties have been reported in numerous experimental[29] and theoretical studies[30, 31].

$$S(\Gamma)=-\frac{2}{\hbar}\mathrm{Im}\int \mathrm{d}r\mathrm{d}t\langle j(r,t)\cdot A^*_{\mathrm{pr}}(r,t)\rangle \quad (5)$$

The ground state geometry was optimized at the Hartree-Fock level with 6-31G(d) basis set using the MOLPRO program[32]. A CASSCF (13o/18e) calculation was used to compute transition current density matrix elements between valence states and to validate our results by comparison with previous studies. Because MOLPRO does not provide the one-body reduced transition density matrix needed to compute the current and charge density matrix elements between different wavefunction symmetries, the transition density matrix elements were calculated for C_1 wavefunction symmetry. Transition current density matrix elements were then computed from the transition density matrix based on the optimized geometry. Nine valence excited states and ten core excited states at the nitrogen K-edge were included for the spectroscopic calculations to match the bandwidth of the incoming pulses. The four degenerate N *1s* molecular orbitals were rotated into the active space to calculate the transition density matrix element between valence and core excited states. Similarly, the single Mg *1s* molecular orbital was rotated into the active space to generate ten core excited states at the Mg K-edge. Our quantum simulation results were consistent with the previous work of Rubio[33] in terms of transition energies, transition dipole moments, and the orbital configuration of each excited state. Note that e_1, e_2, e_3, e_5, and e_7 are optically allowed E_u states, where e_1 and e_2 originate from a doubly degenerate state, while e_3, e_5, and e_7 does not have degenerate pairs within our computation. e_4, e_6, e_8, and e_9 are optically dark states. (See Table S1 and S2 in supporting information for more details)

Results and Discussion

The transition current densities which generate the ring current are shown in Fig. 2. We display three coherences: $\boldsymbol{j}_{e_1e_2}$, $\boldsymbol{j}_{e_4e_9}$, and $\boldsymbol{j}_{e_6e_8}$. These ring currents have the same magnitude and the constant direction of transition current density vectors along the porphyrin ring. e_1 and e_2 are degenerate and belong to

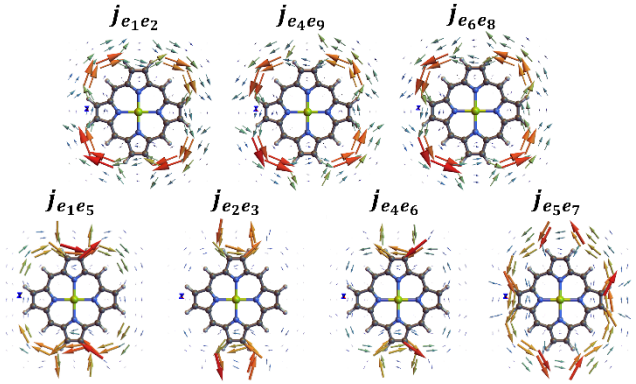

Fig. 2. The transition current density matrix elements in real space which generate the (quasi)ring currents. $\boldsymbol{j}_{e_xe_y}$ is the transition current density between e_x state and e_y state.

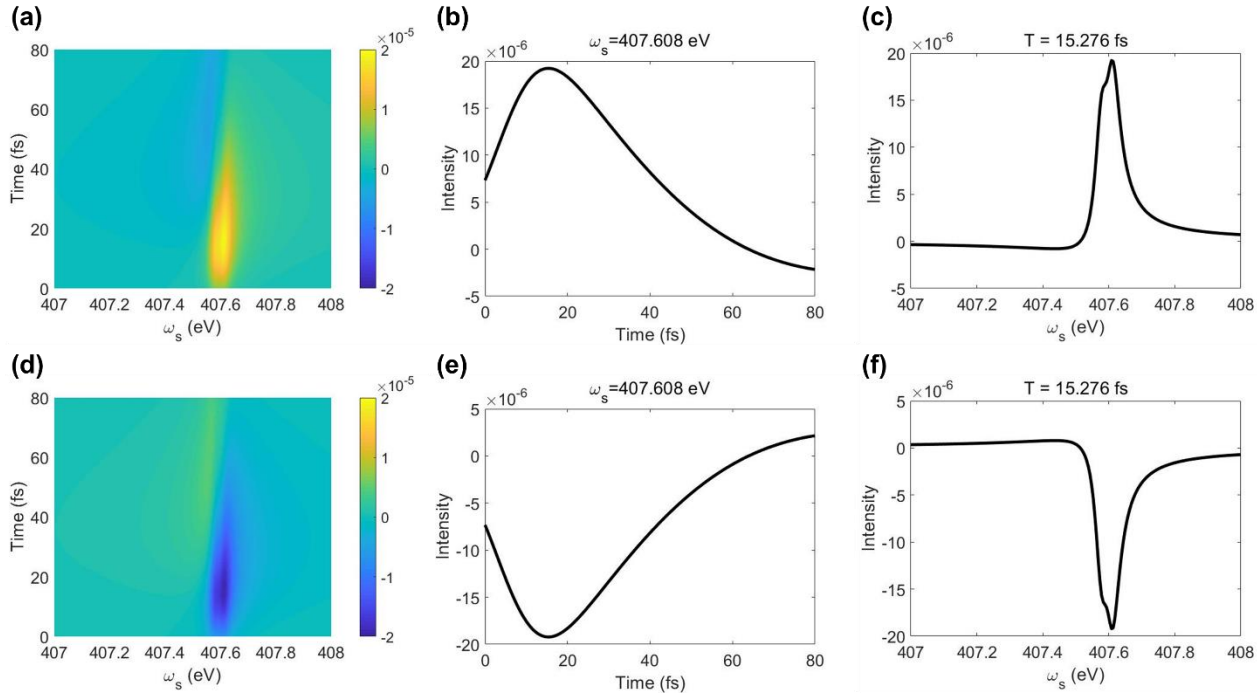

Fig. 3. Top: The TRCD signal calculated for the left (a-c) circularly polarized narrowband light pump. (b) shows the time variation of the TRCD signal along the maximum absolute value of signal. (c) shows the TRCD signal vs probe frequency ω_s. Bottom: same but for right polarized pump

the same E_u symmetry (B_{3u} and B_{2u} for D_{2h}), hence their coherence generates a directional ring current which maintains a clockwise ring current for a long time[34]. In contrast, e_4 and e_8 have A_{2g}/B_{2g} (B_{1g} in D_{2h}) symmetry, while e_6 and e_9 have A_{1g}/B_{1g} (A_g in D_{2h}) symmetry. e_4 and e_9 have a degenerate transition from the same $3B_{3g}$ orbital to degenerate $4B_{2g}$ and $4B_{3g}$ orbitals. Similarly, e_6 and e_8 have a degenerate transition from the same $3B_{2g}$ orbital to degenerate $4B_{2g}$ and $4B_{3g}$ orbitals. Although they have a different wavefunction symmetries, it is possible to generate a ring current by a coherent excitation of two quasi-degenerate excited states with different symmetries[34]. e_6 and e_8 have 0.17 eV splitting and e_4 and e_9 has 0.52 eV splitting, thus $\boldsymbol{j}_{e_4e_9}$ and $\boldsymbol{j}_{e_6e_8}$ generates coherent ring current which shows beating signals by reversing its rotational direction periodically[34], as will be discussed below. Because e_4, e_6, e_8, and e_9 are all optically dark state, we mainly probe the ring current generated by $\langle \boldsymbol{e_1}\, \boldsymbol{e_2} \rangle$ in the following discussions.

There exist quasi-ring current $\boldsymbol{j}_{e_1e_5}$, $\boldsymbol{j}_{e_2e_3}$, $\boldsymbol{j}_{e_4e_6}$, and $\boldsymbol{j}_{e_5e_7}$: they have a constant clockwise ($\boldsymbol{j}_{e_1e_5}$, $\boldsymbol{j}_{e_2e_3}$) or counter-clockwise ($\boldsymbol{j}_{e_4e_6}$, $\boldsymbol{j}_{e_5e_7}$) ring current but the magnitude of vectors differs by and some local vectors exist which do not follow the whole ring current direction. This is apparent for $\boldsymbol{j}_{e_2e_3}$, $\boldsymbol{j}_{e_4e_6}$ where the local ring currents at the top and bottom could be dominating over the vorticity of the whole ring current.

The current density diagonal matrix elements vanish in all cases**.** Eq. 8 shows that the cross product of $\boldsymbol{j}_{ec}(\boldsymbol{k_s}) \times \boldsymbol{j}_{ce}^{\dagger}(-\boldsymbol{k_s})$ is 0. Hence, the TRCD signal originates from electronic coherence, not from populations. The TRCD signal thus directly probes the electronic coherences between electronic states.

The TRCD signals for the left circularly polarized narrowband UV pump (0.1 eV) are shown in Fig. 3a-c. Due to the narrow bandwidth only the coherence $\langle \boldsymbol{e_1}\, \boldsymbol{e_2} \rangle$ contributes to the signal because the Raman pathways of the pump do not contribute to the signal: the only final state available to Raman interaction with the pump is the ground state, where $\boldsymbol{j}_{gc}(\boldsymbol{k_s}) \times \boldsymbol{j}_{cg}^{\dagger}(-\boldsymbol{k_s}) = \boldsymbol{0}$ (*eq* 8). This is confirmed by the oscillatory variation of the TRCD signal (Fig. 3b). The TRCD signal decays slowly after the incident pump is switched off[35] because e_1 and e_2 are almost degenerate (0.03 eV splitting). The coherence between states with large energy splitting will produce fast oscillating signal. The TRCD signal variation with the probe frequency $\boldsymbol{\omega_s}$ (Fig. 3c) shows overlapping double peak near 407.6 eV, reflecting small energy splitting between e_1 and e_2 states and the degeneracy of c_1 and c_2 core states. The contributions from the other core excited states, c_3 to c_{10} are negligibly small and they are invisible in the signal.

Fig. 3d-f present the TRCD signal for the right circularly polarized narrowband UV pump. This signal exhibits the reversed sign but with the same magnitude. The sign of the TRCD signal is thus a direct measure of the direction of the ring current. It also indicates that degeneracy is the key to maintaining long-lasting ring current, because large energy gap will lead to fast oscillating signal. The expectation value of transition current density $\boldsymbol{j}_{e_1e_2}$ in real space vs the pump-probe waiting time is determined by $\boldsymbol{\rho}(\boldsymbol{T})$,

$$\langle \boldsymbol{j}_{e_1e_2}(\boldsymbol{r}, T) \rangle = \sum_{a,b=g,e_1,e_2} \boldsymbol{j}_{ab}(\boldsymbol{r}) \rho_{ba}(T) \qquad (9)$$

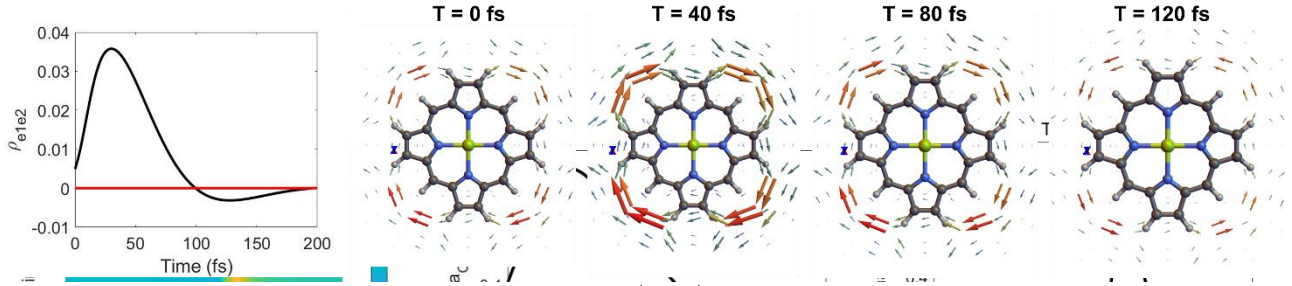

Fig. 4. The expectation value of the transition current density for $\langle e_1\ e_2 \rangle$ coherence, $\boldsymbol{j}_{e_1e_2}$ for several pump-probe waiting times, *T*.

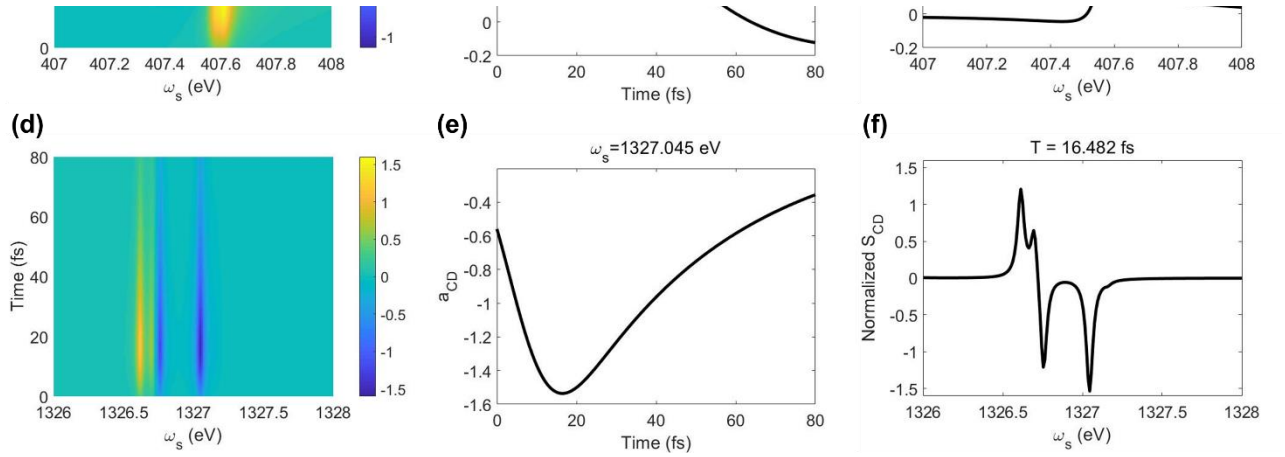

Fig. 5: Comparison of the TRCD asymmetry(a_{CD}), eq. 10, at the N (top, a-c) and Mg (bottom, d-f) K-edges. The asymmetry is larger when probing the magnesium than for the nitrogen atoms.

Fig. 4 shows that $\boldsymbol{\rho}(\boldsymbol{T})$ changes its sign around at 100 fs and 200 fs. The magnitude of the ring current decreases in time and eventually changes its direction from clockwise to counterclockwise at 120 fs. Because the magnitude of the cross product $\boldsymbol{j_{e'c}}(\boldsymbol{k_s}) \times \boldsymbol{j^{\dagger}_{ce}}(-\boldsymbol{k_s})$ is time-independent, the signal will vary with the pump-probe waiting time, $\boldsymbol{T}$. The absolute value of the TRCD signal thus directly reflects the magnitude of the ring current in the real space.

To investigate the element-sensitivity of TRCD in the presence of ring currents, we compare TRCD signals with a probe tuned at the N or Mg K-edges. To compare signals at such different frequency regimes, it is customary to define the CD asymmetry[29] as the ratio between the chiral contribution and the achiral background:

$$a_{\mathrm{CD}}(\omega_s, T) = \frac{S_{\mathrm{abs}}(\omega_s, T, L) - S_{\mathrm{abs}}(\omega_s, T, R)}{1/2\,(S_{\mathrm{abs}}(\omega_s, T, L) + S_{\mathrm{abs}}(\omega_s, T, R))} \qquad (10)$$

where $\boldsymbol{S_{\mathrm{abs}}}$ indicates the absorption amplitude after interaction with left or right circularly polarized X-ray probe pulse.

Note that the static X-ray absorption signal (XAS) cannot be used because it vanishes in the region of the spectrum where the transient appears. The asymmetry ratio would be ill-defined in most regions of the spectra. Thus, we use as a denominator of $\boldsymbol{a_{\mathrm{CD}}}$ the value of the transient absorption in the spectral region of significant CD.

The asymmetry ratios $\boldsymbol{a_{\mathrm{CD}}}$ at the N and Mg K-edge are shown in Fig. 5. The signals display unusually large asymmetry ratios (above 100%) compared to standard CD. This stems from the fact that no static signal (CD and XAS) exists in that spectral region, i.e. the transition from e_1 and e_2 to the core states is made possible only by the actinic pump. Additionally, ring currents of opposite directions induce significant difference in the transient absorption of the X-ray probe. We also observe that the asymmetry ratio is larger for Mg than for N, reaching a maximum of 164% for the former and 110% for the latter. This difference indicates that the Mg atom experiences a higher asymmetry that can be assigned to the larger local magnetic field. The magnetic field created by the ring currents is the physical quantity breaking the parity of the molecular system and reaches its maxima at the ring center.

Fig. 6 depicts the TRCD signal for a broadband UV pump. It is generated by all possible coherences arising from the large bandwidth (1.0 eV) which covers the e_3 to e_9 valence states. The signal variation with time (Fig. 6b) is complex. The signal variation with $\boldsymbol{\omega_s}$ (Fig. 6c) shows peaks near 405.3 and 405.7 eV, which correspond to transitions from e_3, e_5, and e_7 valence excited states to c_1 and c_2 core excited states. Again, the other

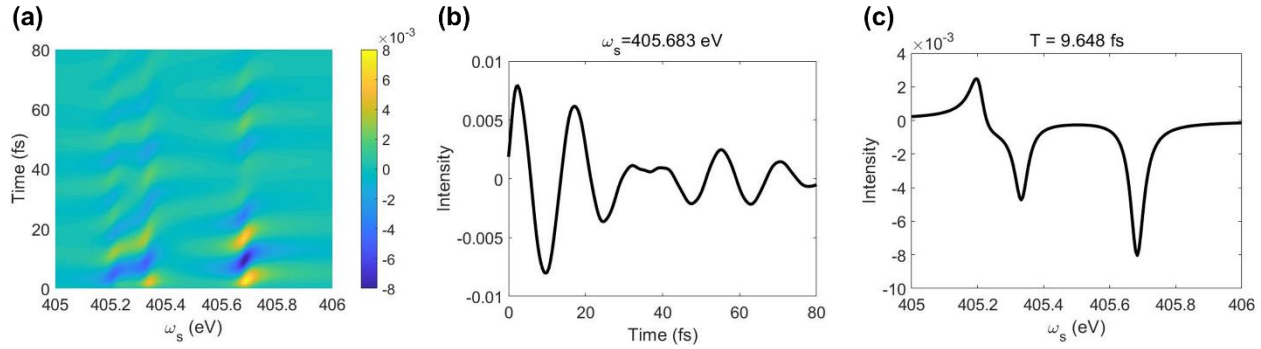

Fig. 6. The TRCD signal calculated for left circularly polarized broadband light pump, where the central frequency was set to the transition energy between the ground and the 5th excited states. (b) and (c) show the time and the probe frequency versus TRCD signal plot along the maximum absolute value of TRCD signal, respectively.

core excitations make negligible contributions to the signal due to their small transition current density. As shown in Fig. 6a, we find two coherences that contribute to the signal.

According to *eq* 8, the signal is determined by $\boldsymbol{\rho_{ee'}(T)}$ and the cross product, $\boldsymbol{j_{e'c}(k_s) \times j^{\dagger}_{ce}(-k_s)}$. $\boldsymbol{\rho_{ee'}(T)}$ for possible coherences are shown in Fig. S4. It shows that the $\boldsymbol{\rho_{e_3e_5}}$, $\boldsymbol{\rho_{e_3e_7}}$, and $\boldsymbol{\rho_{e_5e_7}}$, which are $\langle \boldsymbol{e_3\ e_5} \rangle$, $\langle \boldsymbol{e_3\ e_7} \rangle$, and $\langle \boldsymbol{e_5\ e_7} \rangle$ coherences are dominant. This is because of the large transition dipole moments between the ground state to e_3, e_5, and e_7 valence excited states.

The z component of the cross product $\boldsymbol{j_{e'c}(k_s) \times j^{\dagger}_{ce}(-k_s)}$ is determined by the x component of $\boldsymbol{j_{e'c}}$ and the y component of $\boldsymbol{j^{\dagger}_{ce}}$ and vice versa (Table S3). For e_3, e_5, and e_7 valence excited states, the cross product $\boldsymbol{j_{e_3c}(k_s) \times j^{\dagger}_{ce_5}(-k_s)}$ and $\boldsymbol{j_{e_3c}(k_s) \times j^{\dagger}_{ce_7}(-k_s)}$ are larger than $\boldsymbol{j_{e_5c}(k_s) \times j^{\dagger}_{ce_7}(-k_s)}$ because $\boldsymbol{j_{ce5}}$ and $\boldsymbol{j_{ce7}}$ both has large y component but small x component but $\boldsymbol{j_{ce3}}$ has large x component. Eventually, our signal mostly comes from the coherences $\langle \boldsymbol{e_3\ e_5} \rangle$ and $\langle \boldsymbol{e_3\ e_7} \rangle$ which do not generate a ring current.

In the real system, the e_1, e_3, e_5, and e_7 states are doubly degenerate, i.e. {e_1, $e_{1'}$}, …, {e_7, $e_{7'}$} as reported by quantum calculations with high symmetry[33, 36]. Each coherence between degenerate states generate a ring current. By using broadband pump, the TRCD signal probes multiple coherences which generate multiple ring currents.

It is clearer to use the TRCD signal to measure the ring current when it is accompanied by measurement of the induced magnetic field strength[37] because it can reflect the vorticity of the ring currents. The induced magnetic field at the center of the Mg-porphyrin ($\boldsymbol{x, y, z = 0}$) can be calculated with the Biot-Savart law[23],

$$\boldsymbol{B}(x, y, z = 0) = -\frac{\mu_0}{4\pi}\int\int\int \frac{\vec{j}(x,y,z) \times (-x\vec{x} - y\vec{y} - z\vec{z})dxdydz}{(x^2+y^2+z^2)^{3/2}} \quad (11)$$

where $\boldsymbol{\mu_0}$ refer to the vacuum permittivity, $\vec{x}$, $\vec{y}$, and $\vec{z}$ are the unit vectors along the x, y, and z axis, respectively. The induced magnetic field strengths for the ring-current-generating coherences, $\langle \boldsymbol{e_1\ e_2} \rangle$, $\langle \boldsymbol{e_4\ e_9} \rangle$, and $\langle \boldsymbol{e_6\ e_8} \rangle$ and the ring-current-non-generating coherences $\langle \boldsymbol{e_3\ e_5} \rangle$ and $\langle \boldsymbol{e_3\ e_7} \rangle$ are given in Table 1. The induced magnetic field strength along z direction of the $\langle \boldsymbol{e_3\ e_5} \rangle$ and $\langle \boldsymbol{e_3\ e_7} \rangle$ coherences are 0.0185 and almost 0 T, respectively. In contrast, those of $\langle \boldsymbol{e_1\ e_2} \rangle$, $\langle \boldsymbol{e_4\ e_9} \rangle$, and $\langle \boldsymbol{e_6\ e_8} \rangle$ coherences -0.2578, 0.1349, and 0.2376 T are around 10-20 times higher. The calculated magnetic field strengths are similar to a previous study[6], 0.159 T. However, note that the transition current density in the *eq* 11 does not reflect the small transition dipole moment between the ground state and the dark states (e_4, e_6, e_8, and e_9 states). The generation of the ring current $\boldsymbol{j_{e_4e_9}}$ and $\boldsymbol{j_{e_6e_8}}$ might be possible by the relaxation from the other excited states to these optically dark states. Nevertheless, the measure of induced magnetic field helps to identify the ring current: the sign of the induced magnetic field marks the absolute direction of the ring current, where $\boldsymbol{j_{e_1e_2}}$ is a clockwise current while $\boldsymbol{j_{e_4e_9}}$ and $\boldsymbol{j_{e_6e_8}}$ are counterclockwise ring currents as shown in Fig. 2.

Table 1. The Induced Magnetic Field Strength (in Tesla) for different Coherences, calculated at the center of the Mg-porphyrin.

The type of coherence	Induced magnetic field strength (T)		
	B_x	B_y	B_z
$\langle \boldsymbol{e_1\ e_2} \rangle$	0.0315	-0.0060	-0.2578
$\langle \boldsymbol{e_4\ e_9} \rangle$	-0.0170	0.0046	0.1349
$\langle \boldsymbol{e_6\ e_8} \rangle$	-0.0265	0.0049	0.2376
$\langle \boldsymbol{e_3\ e_5} \rangle$	-0.0030	0.0028	0.0185
$\langle \boldsymbol{e_3\ e_7} \rangle$	0.0001	-0.0007	~0

Fig. 7a and 7d show that the TRCD signals induced by a linearly polarized pump are about 1000 times smaller than one induced by circular polarization. It indicates that the circular polarization is an effective way of generating ring current and induced magnetic field as suggested by the Manz group[6]. It is apparent from the ladder diagram (Fig. 1b) that the linear polarization to x or y axis can excite only e_1 or e_2 from the ground state, hence the cross product $\boldsymbol{j_{e_1c}(k_s) \times j^{\dagger}_{ce_1}(-k_s)}$ or $\boldsymbol{j_{e_2c}(k_s) \times j^{\dagger}_{ce_2}(-k_s)}$ become zero by definition. The $\boldsymbol{\omega_s}$ vs TRCD signal (Fig. 7c and 7f) shows only a single peak, compared to the double peak feature of the circular polarization, indicating that either only e_1 or e_2 state contribute to the TRCD signal. In our simulation, the x or y component of the transition dipole moment of e_1 and e_2 are not exactly zero, but around

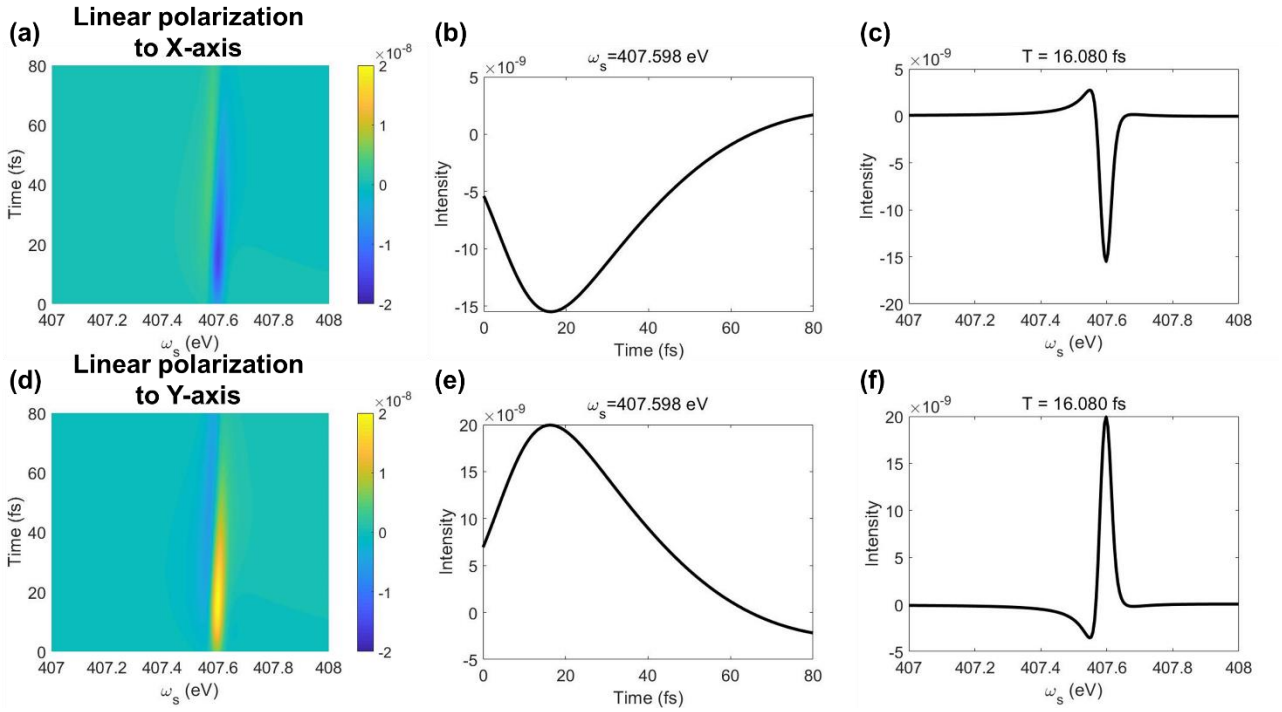

Fig. 7. The TRCD signal calculated for the linearly polarized light pump (a-c: linear polarization to x-axis, d-f: linear polarization to y-axis). (b) and (e) shows the time variation of the TRCD signal along the maximum absolute value of TRCD signal. (c) and (f) show the probe frequency ω_s versus TRCD signal.

1,000 times smaller than their y or x component, making it 1,000 times weaker than the TRCD signals induced by circular polarization.

Pumping with two pulses with x and y components is the same as pumping with a pulse oriented at 45° between x and y a vector and can thus induce a $\langle \boldsymbol{e_1}\, \boldsymbol{e_2} \rangle$ coherence that would give a non-vanishing signal. Indeed, the TRCD is sensitive to coherences in general, of which ring currents are a special case. However, the coherences induced by an x-y pump scheme would not be a signature of a ring current and does not survive a complete or partial rotational averaging. If the molecules are average around the probe (or pump) wavevectors, the pump + molecules have a cylindrical symmetry, and an x-y polarized pump is totally equivalent to an x or y polarized pump. Ring currents in molecules are created by a transfer of angular momentum from the field to the matter[38] and an x-y linearly polarized pulse does not carry such a momentum.

By the same argument, TRCD signal is non-zero when coherences are present in the molecular system whether the system is aromatic or not, as long as the transition dipoles of the two transitions involved in the probe interaction are not pointing in the same direction. However, when a narrowband pump was used, an aromatic ring molecule would have a slow-decaying TRCD signal with larger magnitude while a non-aromatic ring molecule would have a fast-oscillating TRCD signal with much smaller magnitude because the cross product in *eq* 8 is maximized for the degenerate states.

Conclusions

We have shown that time-resolved circular dichroism signals provide a direct measure of the magnitude and the direction of the electronic ring current. These measurements are simpler to interpret than photoelectron CD or high-harmonic-generation spectroscopy. The electronic ring current is generated by the coherent superposition of electronic states induced by circularly polarized light and are tracked by a time-delayed circularly polarized X-ray probe pulse. The signal is calculated using the minimal coupling Hamiltonian which allow to express it directly in terms of the relevant material quantity, transition current densities. TRCD signals obtained from the left and right narrowband circularly polarized light pump have opposite signs, indicating that the signal is a direct signature of the ring current. The absolute value of the signal gives the magnitude of the ring current. The narrowband pump can selectively excite the doubly degenerate excited states to probe a specific ring current or the broadband pump can detect multiple coherences/ring currents at the same time.

X-rays allow to study transient signals in region where no static achiral background is present, leading to extremely large asymmetry ratios for such techniques. Additionally, X-rays can address different sites in the molecules. Here, we have focused on the amplitude of the TRCD signals for different atomic positions (at the center or on the ring), such sensitivity can also provide extra information for systems involving multiple rings with different atoms.

The strength of the induced magnetic field, calculated based on Biot-Savart law, directly reflects the vorticity of an electronic coherence which helps to identify a ring current and its absolute direction. The circular polarization is around 1,000 times more sensitive than linear polarization to probe electronic

coherences. We expect that an aromatic and anti-aromatic molecule will show the opposite TRCD signal under the same circularly polarized light pump. Hence, our direct approach to access the electronic coherences/ring currents opens a window to measure molecular aromaticity[39]. Furthermore, ring currents can be generated and probed by TRCD while a molecule is experiencing an ultrafast nuclear dynamics and can thus be a potential probe for photochemical ring opening or closure reactions.

Conflicts of interest

There are no conflicts to declare.

Acknowledgements

This research was supported by Korea Initiative for fostering University of Research and Innovation Program of the National Research Foundation (NRF) funded by the Korean government (MSIT) (No.2020M3H1A1077095). We wish to thank acknowledge the support of the National Science Foundation through Grant No. CHE-1953045 and of the U.S. Department of Energy, Office of Science, Office of Basic Energy Sciences under Award DE-FG02-04ER15571. S.M was supported by the DOE grant. We gratefully acknowledge Daeheum Cho and Stefano M. Cavaletto for providing their code for calculating and visualizing transition density matrix elements.

Notes and references

1. J. A. N. F. Gomes and R. B. Mallion, *Chem. Rev.*, 2001, **101**, 1349-1384.
2. H. Fliegl, S. Taubert, O. Lehtonen and D. Sundholm, *Phys. Chem. Chem. Phys.*, 2011, **13**, 20500-20518.
3. R. Gershoni-Poranne and A. Stanger, *Chem. Soc. Rev.*, 2015, **44**, 6597-6615.
4. P. v. R. Schleyer, C. Maerker, A. Dransfeld, H. Jiao and N. J. R. van Eikema Hommes, *J. Am. Chem. Soc.*, 1996, **118**, 6317-6318.
5. H. J. Dauben, J. D. Wilson and J. L. Laity, *J. Am. Chem. Soc.*, 1969, **91**, 1991-1998.
6. I. Barth, J. Manz, Y. Shigeta and K. Yagi, *J. Am. Chem. Soc.*, 2006, **128**, 7043-7049.
7. E. Räsänen, A. Castro, J. Werschnik, A. Rubio and E. K. U. Gross, *Phys. Rev. Lett.*, 2007, **98**, 157404.
8. K.-J. Yuan and A. D. Bandrauk, *Phys. Rev. A*, 2013, **88**, 013417.
9. M. Kanno, H. Kono and Y. Fujimura, *Angew. Chem. Int. Ed.*, 2006, **45**, 7995-7998.
10. H. Mineo and Y. Fujimura, *J. Phys. Chem. Lett.*, 2017, **8**, 2019-2025.
11. M. Pawlicki and L. Latos-Grażyński, *Chem.: Asian J.*, 2015, **10**, 1438-1451.
12. G. Merino, T. Heine and G. Seifert, *Chem. Eur. J.*, 2004, **10**, 4367-4371.
13. I. Barth and J. Manz, *Angew. Chem. Int. Ed.*, 2006, **45**, 2962-2965.
14. I. Barth and J. Manz, *Phys. Rev. A*, 2007, **75**, 012510.
15. R. J. Abraham and M. Reid, *J. Chem. Soc., Perkin Trans. 2*, 2002, DOI: 10.1039/B201789J, 1081-1091.
16. J. Juse′lius and D. Sundholm, *Phys. Chem. Chem. Phys.*, 1999, **1**, 3429-3435.
17. K. Jug, *J. Org. Chem.*, 1983, **48**, 1344-1348.
18. A. Soncini and P. W. Fowler, *Chem. Phys. Lett.*, 2008, **450**, 431-436.
19. P. W. Fowler and A. Soncini, *Chem. Phys. Lett.*, 2004, **383**, 507-511.
20. K.-J. Yuan, C.-C. Shu, D. Dong and A. D. Bandrauk, *J. Phys. Chem. Lett.*, 2017, **8**, 2229-2235.
21. M. Wollenhaupt, M. Krug, J. Köhler, T. Bayer, C. Sarpe-Tudoran and T. Baumert, *Appl. Phys. B*, 2009, **95**, 245-259.
22. O. Neufeld and O. Cohen, *Phys. Rev. Lett.*, 2019, **123**, 103202.
23. K. Köksal and F. Koç, *Comp. Theor. Chem.*, 2017, **1099**, 203-208.
24. F. Schotte, M. Lim, T. A. Jackson, A. V. Smirnov, J. Soman, J. S. Olson, G. N. Phillips, M. Wulff and P. A. Anfinrud, *Science*, 2003, **300**, 1944.
25. S. Mukamel, *Principles of nonlinear optical spectroscopy*, Oxford university press New York, 1995.
26. J. J. Rodriguez and S. Mukamel, *J. Chem. Phys.*, 2012, **137**, 205102.
27. O. Roslyak and S. Mukamel, A unified quantum field description of spontaneous and stimulated nonlinear wave mixing and hyper-Rayleigh scattering, EVU Lecture Notes, Lectures of Virtual University, Max-Born Institute, 2010. https://www.semanticscholar.org/paper/A-unified-quantum-field-description-of-spontaneous-Roslyak-Mukamel/5372e87c1a321ee7e59994c863fe9924c67c4302
28. V. Y. Chernyak, P. Saurabh and S. Mukamel, *J. Chem. Phys.*, 2015, **143**, 164107.
29. M. Gouterman, in *The Porphyrins*, ed. D. Dolphin, Academic Press, 1978, DOI: https://doi.org/10.1016/B978-0-12-220103-5.50008-8, pp. 1-165.
30. J. Hasegawa, M. Hada, M. Nonoguchi and H. Nakatsuji, *Chem. Phys. Lett.*, 1996, **250**, 159-164.
31. E. J. Baerends, G. Ricciardi, A. Rosa and S. J. A. van Gisbergen, *Coord. Chem. Rev.*, 2002, **230**, 5-27.
32. H.-J. Werner, P. J. Knowles, G. Knizia, F. R. Manby and M. Schütz, *WIREs Comput Mol Sci.*, 2012, **2**, 242-253.
33. M. Rubio, B. O. Roos, L. Serrano-Andrés and M. Merchán, *J. Chem. Phys.*, 1999, **110**, 7202-7209.
34. H. Mineo, S. H. Lin and Y. Fujimura, *Chem. Phys.*, 2014, **442**, 103-110.
35. K. Nobusada and K. Yabana, *Phys. Rev. A*, 2007, **75**, 032518.
36. D. Sundholm, *Chem. Phys. Lett.*, 2000, **317**, 392-399.
37. P. Kowalska, M. D. Peeks, T. Roliński, H. L. Anderson and J. Waluk, *Phys. Chem. Chem. Phys.*, 2017, **19**, 32556-32565.
38. M. Kanno, H. Kono and Y. Fujimura, *Applied Sciences*, 2018, **8**.
39. I. S. Ulusoy and M. Nest, *J. Am. Chem. Soc.*, 2011, **133**, 20230-20236.

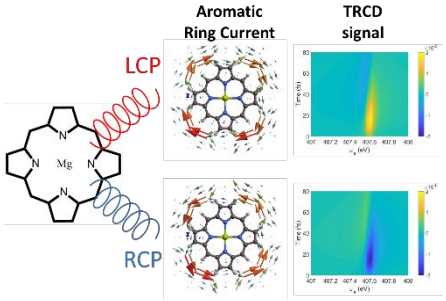

Time-resolved Circular Dichroism signal as a monitor of aromatic ring current in Mg-porphyrin.